Spin coated chitin films for biosensors and its analysis are depended on chitin-surface interactions

Marco G. Casteleijn[#1], Dominique Richardson[1], Petteri K. Parkilla[1], Niko Granqvist[2], Arto Urtti[1,3], Tapani Viitala[1].

1) Drug Research Program, Division of Pharmaceutical Biosciences, Faculty of Pharmacy, University of Helsinki, Finland; 2) BioNavis Ltd., Tampere, Finland, 3) School of Pharmacy, Faculty of Health Sciences, University of Eastern Finland, Kuopio, Finland

Corresponding author: Marco Casteleijn, Division of Pharmaceutical biosciences and the Drug Research Program, University of Helsinki, Viikinkaari 5 E, 00014 University of Helsinki, FINLAND. marco.casteleijn@helsinki.fi

Keywords: Chitin, Surface Plasmon Resonance, Chitin Binding Domain, Split-Inteins, Biosensor, Layer Modeling.

Abstract

Chitin, abundant in nature, is a renewable resource with many possible applications in bioengineering. Biosensors, capable of label-free and in-line evaluation, play an important role in the investigation of chitin synthesis, degradation and interaction with other materials. This work presents a comparative study of the usefulness of a chitin surface preparation, either on gold or on polystyrene (PS). In both cases the most common method to dissolve chitin was used, followed by a simple spin-coating procedure. Multi-parametric surface plasmon resonance (MP-SPR), modeling

of the optical properties of the chitin layers, scanning electron microscopy, and contact angle goniometry were used to confirm: the thickness of the layers, the refractive indices of the chitin layers, the hydrophobicity, the binding properties of the chitin binding domain (CBD) of *Bacillus circulans*, and the split-intein capture process. Binding of the CBD differed between chitin on gold versus chitin on PS in terms of binding strength and binding specificity due to a less homogenous structured chitin-surface on gold in comparison to chitin on polystyrene, despite a similar thickness of both chitin layers in air and after running buffer over the surfaces. The use of the simple method to reproduce chitin films on a thin polystyrene layer to study chitin as a biosensor and for chitin binding studies was obvious from the SPR studies and the binding studies of CBD as moiety of chitinases or as protein fusion partner. In conclusion, stable chitin layers for SPR studies can be made from chitin in a solution of DMA and LiCl followed by spin-coating if the gold surface is protected with PS.

Introduction

Chitin, along with its derivatives, is an increasingly popular biomaterial due to several useful properties, including biodegradability, low immunogenicity, non-toxicity, and biocompatibility [1-3]. Chitin is the main constituent of the exoskeletons of arthropods and is also found in fungal cell walls and it is the second most abundant biopolymer after cellulose [3]. Chitin easily be processed in to a number of derivatives, *e.g.* chitosan; these have shown promising applications in a broad range of areas, including food science, medicine and agriculture [4].

Chitin is an insoluble linear polymer of ß-1,4-linked N-acetylglucosamine residues (figure 1) and three polymorphs of this polysaccharide are known [5]. It exists in three structural forms: α-, ß- and γ-chitin that have different mechanical properties depending on the arrangement of the polymer

chains. The α-form represents an alternating antiparallel arrangement of polysaccharide chains (e.g. crustaceans), the ß-form is a parallel chain arrangement (found e.g. in squid), and in the γ-form two parallel chains statistically alternating with an antiparallel chain (found e.g. in fungi). The α-chitin isomorph is the most abundant form that is formed by: enzymatic polymerization [6], *in*-vitro biosynthesis [7,8], and recrystallization from solution [9].

The use of chitin films as constituents of biosensors have gained interest as the direct study of chitin is important in gaining insight into enzyme degradation pathways, interactions with natural composite materials (e.g., proteins and polysaccharides), and mechanisms behind biocompatibility and biofunctionality [10, 11]. In order to create chitin surfaces with representative properties similar to its natural structure, chitin needs to be dissolved first, and then deposited onto the sensor surface. The most common method to solubilize chitin is the use of DMA and lithium chloride (LiCl). Recrystallizing chitin from a 5% LiCl in DMA solution by precipitation had an essentially crystalline form as the chitin prior to solution (be it the α- or the ß-form), though the α-form can be slightly disordered [12] An alternative method for the solubilization of chitin has been reported, such as using other polar solvents: LiCl/*N*-methyl-2-pyrolidone, chloride dihydrate/methanol [13], and hexofluoroisopropanol (HFIP) [14], or ionic liquids, such as 1-allyl-3-methylimidazolium bromide ([Amim]Br), [C_2mim][OAc], and 1-butyl-3-methylimidazolium acetate [13]. Thin chitin films are interesting for studies of chitinases which can convert chitin into cheap products such as N-acetylglucosamine for biomedical use [2]. Chitin films on silica surfaces by means of spin-coating were 50 nm thin, but rough [15]. Furthermore, a smooth, thin layer of amorphous chitin was obtained after the spin coating of trimethylsilyl chitin onto a silica or gold surface after which the films were regenerated to amorphous chitin [2].

One analytical method, which is highly compatible with thin layers is surface plasmon resonance (SPR). It is a highly sensitive, non-invasive, and label-free technique that is used extensively for surface interaction studies between polymers and proteins [16]. In addition, it has been used to evaluate a chitin-coated surface in the past using ionic liquids as a solvent [2]. However, no simple protocol for the preparation of thin chitin layers using DMA/LiCl as solvent on SPR gold sensors has been established yet.

In this contribution, we demonstrate that the precipitation of chitin using the common DMA/LiCl solvation method onto a gold surface for subsequent SPR analysis poses a challenge due to the surface properties of gold, but can be protected by an additional coating of polystyrene prior to chitin coating. The composition, thickness, available binding surface, surface hydrophobicity, and ability to interact with a CBD of chitin were characterized with multi-parametric surface plasmon resonance (MP-SPR), scanning electron microscopy (SEM), and contact angle goniometer with two different SPR sensors: bare gold and a polystyrene coated gold. The binding constants of a chitin binding domain fused to a split intein and its split intein counterpart were determined for both systems, as well as the differences in behavior of chitin on gold versus polystyrene after spin coating.

Methodology

Materials

Unless specifically mentioned all commercial chemicals (dimethylacetamide (DMA), LiCl, hexofluoroisopropanol (HFIP), EDTA, DTT, NaN_3, triethanolamine hydrochloride (TEA), Tris, sodium chloride, ampicillin, Isopropyl β-D-1-thiogalactopyranoside (IPTG), magnesium chloride) were obtained from Sigma-Aldrich (USA). Reaction buffers and media used were composed as follows: Buffer A: 100 mM TEA, 1 mM EDTA, 1mM DTT, 1mM NaN_3, pH 7.6 (at 25° C). Buffer

100 B: 20 mM TEA, 1 mM EDTA, 1mM DTT, 1mM NaN_3, pH 8 (at 25° C). Buffer C: 20 mM
101 Tris/HCl, 100 mM sodium choride, pH 7.0 (at 25° C). Buffer D: 50 mM Tris/HCl, 50 mM NaCl,
102 pH 8.0 (at 25°C). DNAse and RNAse were obtained from Epicentre (Madison, WI, USA).
103 Phenylmethylsulfonyl fluoride (PMSF) was obtained from ThermoFisher Scientific, USA.
104 EnPressoB medium was obtained from BioSilta Ltd. (U.K); currently available via EnPresso GmbL
105 (Berlin, DE).
106
107 *DNA methods*
108 The eGFP gene from the pEGFP-C1 plasmid (Clontech, USA) was cloned into the pTYB21
109 plasmid, containing the *Sce*VMA1 gene (NEB, USA) to yield the eGFP-*Sce*VMA1 Intein-CBD
110 construct with use of Gibson Assembly® (NEB, USA) according to manufacturer's instructions.
111 The eGFP gene was also cloned into a pMMRSF17 plasmid that contained the NpuDnaE Intein
112 gene in the same way (the full construct was a gift from Hideo Iwai based on Addgene plasmid #
113 20178). In order to generate the CBD-NpuDnaE$_{N\Delta 16}$ gene, the CBD of the chitinase A1 (CBD$_{ChiA1}$)
114 enzyme of *Bacillus circulans* WL-12 was isolated from the pTYB21 plasmid (NEB, USA) using the
115 following primers in a gradient-PCR reaction using Dynazyme II polymerase (ThermoFisher
116 Scientific, USA):
117 '5-GGAATTCCATATGACAAATCCTGGTGTATC-3' and
118 5'-GGATCCGAATTCTTGAAGCTGCCACAA-3' (fragment A) and the NpuDnaE$_{N\Delta 16}$ gene
119 isolated from the pMMRSF17-NpuDnaE with primers
120 5'-GAATTCGGATCCGCCTTAAGCTATGAAACGAA-3' and
121 5'-CGTTAAGCTTATTGAAGCTGCCACAAGG-3' (fragment B). The last primer introduced a
122 mutation (Cys → Ala) at position one of the NpuDnaE$_{N\Delta 16}$ gene and a linker sequence (EFGS)
123 between the CBD and NpuDnaE$_{N\Delta 16}$ in the final construct in pET21a (see below). In order to
124 generate the NpuDnaE$_{C16}$_ eGFP gene, the NpuDnaE$_{C16}$ was isolated from the pMMRSF17-

125 NpuDnaE plasmid using primers 5'-GGAATTCCATATGGGTCATAATTTTGCACTC-3' and
126 5'-CCCTTGCTCCCATATTAGAAGCTATGAAG-3' (fragment C) and the eGFP gene was
127 isolated from pTYB21-eGFP-Intein-CBD plasmid described above with primers
128 5'-TCATAGCTTCTAATATGGTGAGCAAGGGCGA-3' and
129 5'-TTTCAAGCTTTTACTTCTACAGCTCGTCCATGC-3' (fragment D). In an overlap extension
130 gradient-PCR (42° C – 60° C; 15 cycles) fragments A and B were combined with use of Dynazyme
131 II polymerase (ThermoFisher Scientific, USA). Fragments C and D were combined in similar way
132 (38° C - 45° C; 15 cycles). Faint bands in the latter were amplified with PCR and all reactions were
133 cleaned up with NucleoSpin® Gel and PCR Clean-up columns (Macherey-Nagel, DE). The CBD-
134 NpuDnaE$_{N\Delta 16}$ gene and the NpuDnaE$_{C16}$– eGFP gene were then separately cloned into pET21a
135 expression vectors (Novagen, Merck KGaA, USA) after digestion with NdeI and HindIII
136 (ThermoFisher Scientific, USA) and ligation with T4 ligase (ThermoFisher Scientific, USA). The
137 complete DNA sequences of all genes were verified by gene sequencing (GATC, DE). *Escherichia*
138 *coli* NEB5-alpha competent cells (New England Biolabs, USA) were transformed and used for
139 plasmid propagation [17]. Plasmids were then transformed separately to *E. coli* strain BL21(DE3)
140 (Invitrogen, USA) for protein production.
141
142 *Protein expression and purification*
143 Expression of eGFP-*Sce*VMA1 Intein-CBD, CBD-NpuDnaE$_{N\Delta 16}$ and NpuDnaE$_{C16}$-eGFP was
144 carried out in BL21(DE3) *E. coli* cells. First the transformants were grown o/n in LB Medium with
145 100 µg/ml ampicillin and 1% (w/v) glucose at 30°C from glycerol stocks; 2 ml o/n culture was used
146 to inoculate 50 ml of EnPressoB medium [18] with 100 μg/ml ampicillin at 30° C; 225 rpm (1"
147 amplitude shaker) according to manufacturer's instructions in high yield flasks [19]. Cells were
148 induced with 0.4 mM IPTG after 24 h and grown for another 24 h under the same conditions. Cells
149 were separated from the media via centrifugation (16 000 * g for 15 min) and then lysed by freezing

150 o/n at -20° C in the presence of DNAse (2.5 U/ml), RNAse (2.5 U/ml), Lysozyme (15 μg/ml), 0.1
151 mM PMSF (ThermoFisher Scientific, USA), and $MgCl_2$ in buffer D. The insoluble fraction was
152 removed by centrifugation (15 min at 9000 * g). The soluble protein fraction of CBD-NpuDnaE$_{N\Delta16}$
153 was loaded onto a 1 ml HiTrap DEAE FF column (GE healthcare USA) and eluted with buffer D at
154 incremental sodium chloride concentrations (100 mM, 150 mM, 200 mM, 250 mM, 500 mM). The
155 soluble pooled and concentrated protein fractions of NpuDnaE$_{C16}$-eGFP were heated at 70° C for 20
156 min, insoluble proteins removed by centrifugation (15 min; 16 000 *g), and the supernatant loaded
157 onto a size exclusion chromatography (SEC) HiLoad Superdex 200 prep grade filtration column
158 (GE healthcare, USA) using buffer A at 0.5 ml/min and protein fractions collected. The purity of all
159 fractions was evaluated by SDS-PAGE analysis (AnyKd gels, BioRad, USA) and fractions of the
160 target protein size were pooled. Eluate buffer A was replaced by buffer C using a 5kD NMWL
161 membrane at 2800 rpm (Merck-Millipore, USA). Protein concentrations were determined by OD_{280};
162 Molecular weight and the ε was calculated with the ProtParam tool [20]. Hereafter we will
163 abbreviate CBD-NpuDnaE$_{N\Delta16}$ as CBD-IN$_N$ and NpuDnaE$_{C16}$-eGFP as IN$_C$-eGFP.
164
165 *Chitin coating*
166 Chitin was dissolved in DMA and 5% LiCl according to Austin P.R. (1984) [21] at a final
167 concentration of 0.1% (w/v). Bare gold sensors were spin-coated with 100 μl for 60 sec. at 3600
168 rpm; polystyrene coated senors (BioNavis Ltd., Ylöjärvi, Finland) were spin-coated by adding 100
169 μl to the sensor and then after 60 sec. the sensor was spin-coated at 60 sec. at 3600 rpm. The
170 sensors for SPR were used only once and spin-coated immediately before use, since LiCl leached
171 the gold off of the bare sensors after drying for longer periods at 60° C, and subsequent rehydrating
172 (fig. 1).
173 For scanning electron microscopy imaging the sensor was spin-coated prior to placement in
174 the vacuum chamber of the SEM microscope (application chamber) to determine the structure

175 before applying buffer. Sensors were then placed within 10 minutes in a SPR Navi™ 200
176 (BioNavis Ltd., Ylöjärvi, Finland) instrument and buffer was applied to the flow cell area at 20 °C,
177 with a flow rate of 20 µL/min. Samples were allowed to air-dry for at least 15 minutes before SEM
178 imaging of the flow cell area and the areas outside the flow cell under the same conditions.
179
180 *MP-SPR measurements*
181 Measurements were performed with a multi-parameter SPR Navi™ 200 (BioNavis Ltd., Ylöjärvi,
182 Finland) instrument. The setup was equipped with two incident laser wavelengths, 670 nm and
183 785 nm, two independent flow channels, inlet tubing and outlet (waste) tubing. Both of the flow
184 channels were measured in parallel with 670 nm and 785 nm incident light. The measurement
185 temperature was kept constant at 20 °C. The chitin coated SPR sensors were placed in the flow-cell
186 and SPR spectra were recorded in air after which buffer B was introduced into the flow-cell; the
187 flow rates used for the CBD-IN_N interaction with chitin and for IN_C-eGFP interaction with CBD-
188 IN_N were 20 µL/min. Chitin layer data in air was fitted in LayerSolver 1.2.1 (BioNavis, FIN) with
189 default parameters and simulation mode 0 for the Au layer, and mode 2 for all other layers. The
190 buffer (due to the presence of EDTA) prevented damage to the bare-gold sensors during the SPR
191 measurements due to removal of LiCl. The chitin coated gold and polystyrene sensor slides were
192 first subjected to buffer B for 10 – 30 min until a stable baseline was achieved. In the second phase,
193 CBD-IN_N was injected into both flow channels for 8 minutes at increasing concentrations (490, 981,
194 1961, 3922, 7854 nM, equivalent to 10, 20, 40, 80, 160 ug/ml) to determine the binding constants
195 for both systems. Based on these results, CBD-IN_N was bound to the new chitin coated sensors at
196 0.5 and 5 μg/ml of protein during a 5-minute injection. IN_C-eGFP protein was then injected in both
197 channels for 5 minutes at increasing concentrations (17.5, 175, 350, 701, 1401, 2803 nM, equivalent
198 to 0.5, 5.0, 10.0, 20.0, 40.0, and 80.0 μg/ml) to determine the binding constant of the split-intein
199 pair for both SPR sensors. The data was fitted in TraceDrawer software v1.6 (BioNavis, FIN &

Ridgeview Instruments, SWE) according to the OneToTwo model to obtain the association rates, dissociation rates, and the binding constants after evaluations of other relevant models.

Scanning Electron Microscopy

SEM images were recorded using an FEI Quanta 250 Field Emission Gun Scanning Electron Microscope under high vacuum ($< 6 \times 10^{-4}$ Pa) to prevent deterioration of the chitin layer due to moisture in the air.

Contact angle measurements

Au, PS, Au-chitin, and Au-PS-chitin surfaces were prepared as described above. The Au sensor surface was cleaned in two ways: (1) plasma treated as above and (2) boiled for 15 min in and NH_3 (30%)/H_2O_2 (30%)/H_2O (1:1:5, v/v) oxidizing solution. A syringe and needle were washed with 70% ethanol and rinsed with fully deionized water (Milli-Q water) and the camera was adjusted before each measurement. The shape of the water droplet on the surface was recorded with a CAM 200 optical contact angle meter (KSV instrument LTD) equipped with CCD video camera module and the drop volume was constant during the whole measurement (static mode). The drop height prior to the measurement was 200 pixels (approx. 8 μl of Milli-Q water), and recording started automatically upon detection of the drop on the surface with a frame interval of 1 second for 60 frames. Contact angels were calculated according to the Young-Laplace fitting model using the Attension theta 4.1.0 software (KSV instruments LTD). After the contact angle was stable (i.e. in the case of Au and PS) with out chitin) the mean of frames from 45 second to 60 second was calculated. For the contact angle of water on the chitin surfaces (dry or wet) the rate of the contact angle change was different, but lower than 1° at the end of each measurement.

Result and Discussion

225

226 **Surface properties of the spin coated sensors**

227 We observed in polystyrene (PS) 96-well plates with (a) 0.1% chitin solution in DMA/5% LiCl and
228 (b) 0.1% chitin solution in HFIP [14], and subsequently dried overnight in an oven with a fan at 60°
229 C, that (i) chitin precipitated out of DMA/5% LiCl formed large crystal structures and that non-
230 reproducible amounts remaining in the wells after washing with vigorously with water, (ii) chitin
231 precipitated out of HFIP formed a layered gel, which after upon adding water detached from the PS
232 surface, (iii) eGFP-intein-CBD (IMPACT^{TM} kit [22], New England Biolabs, USA) was able to bind
233 and release eGFP according to the kit instructions from crude cell lysates (data not shown). We also
234 used the eGFP-intein-CBD crude lysate to determine that the CBD does not bind to Au (data not
235 shown). Therefore, in order to study chitin binding and the binding/release of split-inteins, SPR Au
236 sensors coated with chitin were initially dried overnight at 60° C. However, the gold was leached
237 from the retrieved SPR sensors after the experiment (i.e. the gold and chitin layer detached from the
238 glass surface; figure 2). For this reason all binding experiments here reported were performed with
239 buffer B in order to scavenge the LiCl from the surface. In addition, PS coated Au SPR sensors
240 were utilized as well and directly compared.

241

242 The cleaning protocol of gold has an effect on the hydrophobicity of the surface (table 1). Au
243 surfaces boiled for 15 min in a NH_3 (30%)/H_2O_2 (30%)/H_2O (1:1:5, v/v) oxidizing solution were
244 more hydrophobic than plasma cleaned surfaces. Since it had been shown that: (i) more oxidized
245 gold surfaces are more hydrophilic [23], and (ii) the intention of spin-coated chitin is to interact
246 with its surface more effectively by sampling more hydrogen bonds outside its internal structure
247 [24,25] all surfaces were plasma treated prior to spin coating. The polystyrene surface can be easily
248 oxidized through plasma treatment [26].

249

The hydrophobicity of the surfaces was evaluated with a goniometer to determine the contact angle of a water droplet during the first 60 seconds of contact. The chitin surfaces were either spin-coated and then dried under a nitrogen flow or spin-coated, wetted with a few drops of buffer B and then dried under a nitrogen flow (Chitin in air or Chitin in buffer in table 1 respectively). On the Au and PS surfaces the water droplet formed was stable throughout the measurement (figure 3), while the water droplet on pre-wetted chitin surfaces immediately spread over the surface. On dried chitin surfaces the water droplet behaved differently than on the Au-chitin surface or the PS-chitin surface. In Au-chitin the contact angle decreased under 10° after 2 seconds and reached a value below 1° within 30 seconds, while the contact angle of a water droplet on PS-chitin was initially higher, the droplet spread slower, and a thicker water layer remained (figure 3).

The thickness of the chitin layers directly after spin-coating was determined with SPR in air (table 1 & figure 4) by using the Layersolver software based on Granqvist *et al*. [27]. First the Au layer was measured and modeled (figure 4A) after which chitin was spin-coated on the surface and the thickness determined. Due to the high thickness waveguide-fitting for one wavelength would suffice, but the measured SPR spectra at both wavelengths fit the models well. Therefore we always fitted both wavelengths in one model to enhance accuracy. The PS coated Au sensor was determined in similar fashion: first the thickness of PS was determined, after which similar model parameters of the chitin on Au-model were applied to obtain the Au-PS models in air. From the models it is clear that the layer's refractive indices (n) in air are much lower than reported for shrimp chitin, which is reported at $n = 1.61$ [18]. This behavior has previously been observed for spin-coated chitin for which the refractive index can vary greatly between $n = 1.30 - 1.47$ depending on the solvent used [29].

In order to determine the refractive index of chitin after the introduction of buffer, the total internal reflection (TIR) angle was manually fitted in the Layersolver software for the Au-chitin layer. Based on the principle that the bulk effect in the SPR curves is constant, while we assume the Au layer to be constant, the changes in the TIR angle-shape during the stabilization of the TIR angles and overall SPR signal are indicative to the changes in thickness. In addition, it is known that hydrogels, such as polyacrylamide gels have a lower refractive index than the starting material [30]. We observed a hydrated state after washing the spin-coated chitin surface with buffer B prior to the contact angle measurements (fig. 3). Overall, the refractive index of chitin can differ greatly depending on how the polymers are precipitated [29]. We disagree with the assumption of Kittle *et al*. [2] that the refractive index of chitin is 1.51 and thus we used the change of the shape of the TIR angle to fit the theoretical maximum thickness (fig. 5) and a resulting *n*-value for both wavelengths for the Au-chitin layer. Thereafter, we fitted the minimal thickness and refractive index for the experimentally SPR curves manually with the Layersolver software. The results are a realistic range of the thickness and refractive indices for both wavelengths. Since we did not observe the phenomena of the TIR angle-shape changing after the introduction of buffer B over time regarding the Au-PS-chitin surface, we took the minimum and maximum refractive indices determined with the Au-chitin models in buffer, and used them as initial values to manually fit the experimental data as above to find a realistic range of the thickness and *n*-values for the Au-PS-chitin layer in buffer. All four resulting models fit the experimental data the best (fig. 4C and 4F). In addition, an apparent change in the thickness of the PS layer had to be corrected for in the models. Therefore we fitted the sensor parameters simultaneously with the layer (table 1). It is known that DMA damages PS [31], however as we observed in Scanning Electron Microscopy (SEM) imaging (fig. 8C and 8D), enough PS has remained during the short period of interaction with DMA in the spin-coating process. Since DMA is removed during spin-drying [32] and the PS is not severely damaged during

298 the spin-coating process, the deposited LiCl on the surface is not interacting with Au as observed in
299 figure 8C.
300
301 Upon further visual inspection with SEM of the spin coated chitin layers, at first glance chitin on
302 gold or chitin on PS before SPR measurements appear to have similar structures, though appear to
303 be cruder on the Au-PS layer (fig. 8A and 8B). However, after one hour under normal atmospheric
304 conditions at room temperature, chitin on gold presented large build-up structures not observed in
305 the Au-PS layer. As seen in figure 2, this is most likely the result of the electrochemical reaction
306 between Au and Li [33]. In order to remove the LiCl from the dried chitin layer, EDTA was added
307 to a buffer (Buffer B). The response in the SPR sensorgram upon introduction of the liquid phase in
308 either buffer D (without EDTA) or Buffer B (including EDTA) containing buffer differed. Upon
309 contact with buffer D, the base line in the SPR sensorgram sloped slowly down and stabilized after
310 15-20 minutes. In the case of the EDTA containing buffer the baseline dropped immediately and
311 then stabilized within 20 minutes on the Au surface due to changes in the thickness (fig. 5), while
312 the baseline is stable within seconds on the Au-PS surface. The SPR senors with a stable baseline in
313 buffer B were then transferred, while air-drying, within 15 minutes to the vacuum chamber of the
314 SEM equipment (fig. 8E and 8F). The cubical structures on the Au-PS surface are clearly sodium
315 chloride crystals [34], while it is unclear what the large macrostructures are on the Au surface at
316 this magnification. In-between the macrostructures chitin can be seen at higher magnification (fig.
317 8G and 8I). On Au, chitin appears to be connected at the edge of the macrostructures (fig. 8G
318 arrow), while chitin on the Au-PS surface appears to be more uniform.
319
320 Chitin responded to the atmospheric conditions rather rapidly, most likely due to moisture in the air,
321 since when the Au-PS surface was directly placed in vacuum (< 30 seconds; fig. 9A and 9C) or
322 after 5 minutes (fig. 9B and 9D), the spin-coated surfaces looked very different. At lower

magnification we observed geometric patterns appear after a few minutes (fig. 9B), which were stable on the Au-PS surfaces for at least an hour (fig. 8B). At higher magnification we observed a flakey structure (fig. 9C) at first and a more uniform geometrical surface of the spin-coated surface after 5 minutes (fig. 9D).

The chitin layers on Au or Au-PS in air were similar when observed with SEM and their layer thickness was nearly the same. The differences after exposure of buffer B, at a flow of 20 μL/min in the SPR flow-cell, were evident; while the surface of Au looks damaged and not uniform, chitin on Au-PS appears smoother. The predicted range of the chitin layer's thickness on Au-PS was slightly lower that chitin on Au. Our layers were in the same range as earlier reported thicknesses [2].

Differences in binding properties

The surfaces (Au spin-coated with chitin and Au coated with PS and spin-coated with chitin) did not only differ in surface properties, the chitin binding domain of *Bacillus circulans* (CDB_{ChiA1}) showed different binding characteristics to chitin as well (table 2 & figure 6). CDB_{ChiA1} fused to the split-intein $NpuDnaE_{N\Delta16}$ (CBD-IN_N) was titrated to both surfaces at increasing concentrations (figure 6). The resulting sensorgrams were then fitted to different models using the TraceDrawer software until the best fit with the lowest variation (Chi-Square) was calculated. For both experiments the best fitting model was a OneToTwo model [35]. This model indicates that the CBD-IN_N protein binds specifically and nonspecifically to the chitin surface.

The chitin-binding domain bound very tightly to both chitin layers and we did not observe a dissociation phase, however there was a clear difference in binding to spin-coated chitin on gold versus spin-coated chitin on a thin polystyrene layer. Not only was the binding of the CBD to chitin on PS must stronger, the binding rates were higher, and were more specific (table 2 and figure 6).

348

349 The binding constants for various CBDs have been mainly determined by means of solution
350 depletion studies and ICT (table 3). Though the theoretical differences between the solution
351 depletion method and SPR had been thoroughly described [36,37], to the best of our knowledge we
352 could find only one direct comparison of both methods of a protein interaction with a
353 polysaccharide: the study of BSA binding to cellulose. When the binding constant of BSA to
354 cellulose was determined by isothermal titration calorimetry (ITC) and the solution depletion
355 method at pH 7-7.5, the authors [38] found a K_d of 10 μM or 0.66 mg/ml by ICT and 38 μM or 2.53
356 mg/ml by solution depletion followed by UV spectroscopy, with a B_{max} of 0 (ICT) or 36.3 mg
357 (solution depletion & UV) BSA/gram cellulose extrapolated from their graphs for 0% pyridinium-
358 grafted chitin nanocrystals, while in an earlier SPR study [39], at pH 7-7.5, about 0.5 mg/cm^2 was
359 bound to the sensor surface. This was an equivalent to a B_{max} of about 0.018 mg BSA/gram of
360 cellulose. The binding kinetics were not determined. The B_{max} determined with ICT of zero is close
361 to the value determined with SPR and the difference may in the margin of error. The B_{max}
362 determined with the solution depletion method was over 2000-fold higher than with SPR. Though
363 the ease of the solution depletion method cannot be denied, SPR offers a more detailed analysis of
364 the surface properties and is more sensitive. On the other hand, as pointed out by Lombardo *et al.*
365 [38], during SPR measurements, a constant flow of BSA is supplied over immobilized cellulose,
366 forcing the protein to adsorb to a higher extent. ITC seems to be closer in correlation with SPR than
367 the depletion method. Therefore, when comparing the values in table 3 derived from the solution
368 depletion method with SPR, we can expect lower K_d values with at least one order of magnitude. In
369 addition, as determined by Hashimoto *et al.* [44], CBD_{CHA1} binds only to insoluble chitin. This may
370 explain the even higher affinity (i.e. smaller K_d) in the case of chitin spin-coated on the polystyrene
371 surface, since the chitin layer formed a stable, uniform layer immediately upon the introduction of
372 buffer B.

373

374 The chitin structure had an effect on its interaction with CBD-IN_N and IN_C-eGFP. Though in both
375 the Au-chitin and the Au-PS-chitin surface the CBD-IN_N and IN_C-eGFP interaction followed a
376 capture and collapse mechanism the kinetic data fitting of our SPR experiments (Fig. 7) confirmed
377 by the observation of the single binding phase observed with stopped-flow fluorescence [40]. The
378 calculated binding constants were higher for the Au-chitin surface, but with a higher specific
379 binding. On the other hand, on the Au-PS-chitin surface, the intein pair bound more tightly, but
380 showed some non-specific binding as well. The binding constant of the split intein pair was in
381 general higher than observed previously, except for Au-PS with a 0.25 nM CBD-IN_N solution
382 titrated to the surface, before introduction of the split intein pair: 1.2 nM [40] and 1.6 nM (this
383 study; table 2).

384

385 **Conclusions**

386 In summary, this work highlights the differences between two different sensor chips and their
387 implication for the study of chitin binding proteins and chitin binding domain as an immobilizing
388 agent for the study of split-inteins. The spin-coated films of chitin using with DMA/LiCl as a
389 solvent is damaging for the gold layer, despite the use of EDTA in the SPR running buffer.
390 Polystyrene on a gold sensor protects the gold layer from the solvent well enough for a
391 homogeneous chitin layer to form during the spin-coating process. SPR is a suitable tool to
392 determine the thickness of the spin-coated layers before applying buffer, during the introduction of
393 buffer to the system, and to investigate the binding behavior of protein binding to the sensors. The
394 utility of chitin films as biosensors is evident from the chitin binding domain binding studies. These
395 results are expected to enable studies of chitin layer properties and interactions with biomolecules
396 without the use of labels in real-time with high sensitivity.

397

Acknowledgments

This work was funded and supported by the Academy of Finland projects 272597, 303884, and 137053. We thank Dr. Hideo Iwai for providing us with the plasmid containing the NpuDnaE gene. We thank Dr. Ilya Belevich from the Electron Microscopy Unit, Institute of Biotechnology, of the University of Helsinki, Finland for his technical guidance with scanning electron microscopy and image analysis. We also would like to thank Erja Piitulainen and Leena Pietilä for their kind laboratory assistance, and Regina Casteleijn-Osorno of AaltoEE and Dr. Alex Bunker of the Drug Research Program at the University of Helsinki for comments that greatly improved the manuscript.

References

1. C.K.S. Pillai, W. Paul, C.P. Sharma, Chitin and chitosan polymers: Chemistry, solubility and fiber formation, Prog. Polym. Sci. 34 (2009) 641–678.
2. J.D. Kittle, C. Wang, C. Qian, Y. Zhang, M. Zhang, M. Roman, J.R. Morris, R.B. Moore, A.R. Esker, Ultrathin Chitin Films for Nanocomposites and Biosensors, Biomacromolecules, 13 (2012) 714–718. DOI: 10.1021/bm201631r
3. M.N.V.R. Kumar, A review of chitin and chitosan applications, React. Funct. Polym. 46 (2000), pp. 1 – 27.
4. B.K. Park, M.M. Kim, Applications of Chitin and Its Derivatives in Biological Medicine. Int. J. Mol. Sci., 11(12) (2010) 5152–5164 http://doi.org/10.3390/ijms11125152
5. P. Jolles, R.A.A. Muzzarelli, Chitin and Chitinases. Jollès P, Muzzarelli RAA, editors. Birkhauser Verlag; Basel, Switzerland, 1999.
6. J. Sakamoto, J. Sugiyama, S. Kimura, T. Imai, T. Itoh, T. Watanabe, S. Kobayashi, Artificial chitin spherulites composed of single crystalline ribbons of α-chitin via enzymatic polymerization. Macromolecules. 33 (2000) 4155–4160.

7. J. Ruiz-Herrera, V.O. Sing, W.J. van der Woude, S. Bartnicki-Garcia, Microfibril assembly by granules of chitin synthetase. Proc. Natl. Acad. Sci. USA, 72 (1975) 2706–2710.
8. S. Bartnicki-Garcia, J. Persson, H. Chanzy, An electron microscope and electron diffraction study of the effect of calcofluor and congo red on the biosynthesis of chitin *in vitro*. Arch. Biochem. Biophys. 310 (1994) 6–15.
9. W. Helbert, J. Sugiyama, High-resolution electron microscopy on cellulose II and α-chitin single crystals, Cellulose, 5 (1998) 113–122.
10. G. Vaaje-Kolstad, B. Westereng, S.J. Horn, Z. Liu, H. Zhai, M. Sørlie, V.G.H. Eijsink, Science, 330 (2010) 219–222.
11. S. Boddohi, M.J. Kipper, Engineering Nanoassemblies of Polysaccharides, Adv. Mater. 22 (2010) 2998–3016.
12. B. Focher, A. Naggi, G. Torri, A. Cosani, M. Terbojevich, Structural differences between chitin polymorphs and their precipitates from solutions—evidence from CP-MAS C-NMR, FT-IR and FT-Raman spectroscopy, Carbohydr Polym., 17 (1992) 97–102.
13. X. Shen, J. L. Shamshina, P. Berton, G. Gurauc and R. D. Rogers, Hydrogels based on cellulose and chitin: fabrication, properties, and applications, Green Chem., 18 (2016) 53-75.
14. C. Zhong, A. Cooper, A. Kapetanovic, Z. Fang, M. Zhang and M. Rolandi, A facile bottom-up route to self-assembled biogenic chitin nanofibers. Soft Matter, 6 (2010) 5298–5301.
15. Y. Kikkawa, H. Tokuhisa, H. Shingai, T. Hiraishi, H. Houjou, M. Kanesato, T. Imanaka, T. Tanaka, Interaction Force of Chitin-Binding Domains onto Chitin Surface, Biomacromolecules. 9 (2008) 2126– 2131.
16. R.B.M. Schasfoort, A.J. Tudos, Handbook of Surface Plasmon Resonance, The Royal Society of Chemistry, Cambridge, 2008.
17. J. Sambrook, D.W. Russell, Molecular cloning. A laboratory manual, 3rd edition, Cold spring harbor laboratory press, 2001.

18. J. Panula-Perälä, J. Šiurkus, A. Vasala, R. Wilmanowski, M.G. Casteleijn, P Neubauer, Enzyme controlled glucose auto-delivery for high cell density cultivations in microplates and shake flasks, Microbial Cell Factories, (2008) 7, 31. http://doi.org/10.1186/1475-2859-7-31
19. K. Ukkonen, A. Vasala, H. Ojamo, P. Neubauer, High-yield production of biologically active recombinant protein in shake flask culture by combination of enzyme-based glucose delivery and increased oxygen transfer. Microbial Cell Factories, (2011) 10, 107. http://doi.org/10.1186/1475-2859-10-107
20. E. Gasteiger, C. Hoogland, A. Gattiker, S. Duvaud S, M.R. Wilkins, R.D. Appel, A. Bairoch, Protein Identification and Analysis Tools on the ExPASy Server, (In) John M. Walker (ed): The Proteomics Protocols Handbook, Humana Press, 2005, pp. 571-607
21. P.R. Austin. Chitin solvents and solubility parameters. J.P. Zikakis (Ed.), Chitin and chitosan and related enzymes, Academic Press, Inc., Orlando, 1984, pp. 227-237
22. S. Chong, F.B. Mersha, D.G. Comb, M.E.Scott, D. Landry, L.M. Vence, F.B. Perler, J. Benner, R.B. Kucera, C.A. Hirvonen, J.J. Pelletier, H. Paulus, M.Q. Xu, Single-column purification of free recombinant proteins using a self-cleavable affinity tag derived from a protein splicing element, Gene, 192, (1997) 271-281. Doi: 10.1016/S0378-1119(97)00105-4.
23. K. W. Bewig, W. A. Zisman, The Wetting of Gold and Platinum by Water, J. Phys. Chem., 69 (1965) 4238-4242. DOI: 10.1021/j100782a029
24. V.L. Deringer, U. Englert, R. Dronskowski, Nature, Strength, and Cooperativity of the Hydrogen-Bonding Network in α-Chitin, Biomacromolecules, 17 (2016) 996-1003. DOI: 10.1021/acs.biomac.5b01653
25. T. Kameda, M. Miyazawa, H. Ono, M. Yoshida, Hydrogen Bonding Structure and Stability of α-Chitin Studied by ^{13}C Solid-State NMR. Macromol. Biosci., 5 (2005) 103–106. doi:10.1002/mabi.200400142

26. C. C. Dupont-Gillain, Y. Adriaensen, S. Derclaye, P. G. Rouxhet, Plasma-Oxidized Polystyrene: Wetting Properties and Surface Reconstruction. Langmuir, 16 (2000) 8194-8200. DOI: 10.1021/la000326l
27. N. Granqvist, H. Liang, T. Laurila, J. Sadowski, M. Yliperttula, T. Viitala, Characterizing Ultrathin and Thick Organic Layers by Surface Plasmon Resonance Three-Wavelength and Waveguide Mode Analysis. Langmuir, 29 (2013) 8561-8571. DOI: 10.1021/la401084w
28. D.E. Azofeifa, H.J. Arguedas, W.E. Vargas, Optical properties of chitin and chitosan biopolymers with application to structural color analysis, Optical Materials, 35 (2012) 175-183.
29. K. Manabe, C. Tanaka, Y. Moriyama, M. Tenjimbayashi, C. Nakamura, Y. Tokura, T. Matsubayashi, K.H. Kyung, S. Shiratori, Chitin Nanofibers Extracted from Crab Shells in Broadband Visible Antireflection Coatings with Controlling Layer-by-Layer Deposition and the Application for Durable Antifog Surfaces, *ACS App. Mat. & Inter.*, 8 (2016) 31951-31958.
30. J. Franklin, Z.Y. Wang, Refractive Index Matching: A General Method for Enhancing the Optical Clarity of a Hydrogel Matrix. Chem. Mat. 14 (2002) 4487-4489.
31. Labware chemical resistance table, ThermoFisher Scientific, https://tools.thermofisher.com/content/sfs/brochures/D20480.pdf (accessed 30.09.2017)
32. K. Norrman, A. Ghanbari-Siahkalia, N.B. Larsena, 6 Studies of spin-coated polymer films, Annu. Rep. Prog. Chem., Sect. C: Phys. Chem., 101 (2005) 174-201. Doi: 10.1039/B408857N.
33. A Zhiyuan Zeng, W.I. Liang, Y.H. Chu, H. Zheng, *In situ* TEM study of the Li–Au reaction in an electrochemical liquid cell. *Faraday Discuss.*, 176 (2014) 95-107.
34. R. Tran, E. Naseri, A. Kolasnikov, X. Bai, Y. Yang, A new generation of sodium chloride porogen for tissue engineering. Biotechnol. Appl. Biochem., 58 (2011) 335–344.
35. S. Bondza, E. Foy, J. Brooks, K. Andersson, J. Robinson, P. Richalet, J. Buijs, Real-time Characterization of Antibody Binding to Receptors on Living Immune Cells. Frontiers in Immunology, (2017), 8, 455 -. Doi: 10.3389/fimmu.2017.00455

496 36. V. Hlady, J. Buijs, H.P. Jennissen, Methods for Studying Protein Adsorption. Methods in
497 Enzymology, 309 (2011), 402–429.
498 37. E.A. Vogler, Protein Adsorption in Three Dimensions. Biomaterials, 33 (2012) 1201–1237.
499 38. S. Lombardo S, S. Eyley, C Schütz, H. van Gorp, S. Rosenfeldt, G. Van den Mooter, W.
500 Thielemans, Thermodynamic Study of the Interaction of Bovine Serum Albumin and Amino
501 Acids with Cellulose Nanocrystals. Langmuir, 33 (2017), 5473-5481.
502 39. H. Orelma, I. Filpponen, L.S. Johansson, J. Laine, O.J. Rojas, Modification of Cellulose Films
503 by Adsorption of CMC and Chitosan for Controlled Attachment of Biomolecules,
504 Biomacromolecules, 12 (2011) 4311-4318.
505 40. N.H. Shah, E. Eryilmaz, E.D. Cowburn, T.W. Muir, Naturally Split Inteins Assemble through a
506 "Capture and Collapse" Mechanism. J. Am. Chem. Soc. 135 (2013) 18673-18681.
507 41. G. Vaaje-Kolstad, S.J. Horn, D.M.F. van Aalten, B. Synstad B, V.G.H. Eijsink, The Non-
508 catalytic Chitin-binding Protein CBP21 from Serratia marcescens Is Essential for Chitin
509 Degradation. *J. Biol. Chem.*, 280 (2005) 28492.
510 42. K. Manjeet, P. Purushotham, C. Neeraja, A.R. Podile, Bacterial chitin binding proteins show
511 differential substrate binding and synergy with chitinases, Microbiol. Res. 168 (2013) 461-468.
512 43. Z. Li, C. Li, K. Yang, L. Wang, C. Yin, Y. Gong, Y. Pang, Characterization of a chitin-binding
513 protein GP37 of Spodoptera litura multicapsid nucleopolyhedrovirus, Virus Res. 1-2 (2003)
514 113-122.
515 44. M. Hashimoto, T. Ikegami, O. Seino, N. Ohuchi, H. Fukada, J. Sugiyama, T. Watanabe,
516 Expression and Characterization of the Chitin-Binding Domain of Chitinase A1 from Bacillus
517 circulans WL-12. *J. of Bact.* 182 (2000) 3045–3054.
518 45. M. Hardt, R.A. Laine, Mutation of active site residues in the chitin-binding domain
519 ChBDChiA1 from chitinase A1 of Bacillus circulans alters substrate specificity: use of a green
520 fluorescent protein binding assay. *Arch. Biochem. & Biophys.*, 426 (2004) 286-297.

46. K. Somjit, K. Hara, M. Yoshimura, N. Matsuo, O. Kongpun, Y. Nozaki, Effect of shrimp chitin and shrimp chitin hydrolysate on the state of water and dehydration-induced denaturation of lizard fish myofibrillar protein. Food Sci. Technol. Res. J., 11 (2005) 106-114.

Tables

Table 1. Surface properties of the SPR chips, before and after coating.

Layer	Thickness [nm]	n_r (670/785 nm)	Contact angle (at 1 sec/end)[1] [°]
Au (in air)	50.88	0.2033/0.1978	20.7/21.2[2]
			54.5/53.4[3]
Au-chitin (in air)	1910	1.3908/1.3885	15.6/<1
Au-chitin (in buffer)	49.2	1.3617/1.3595	<1/<1[4]
	188.5	1.3463/1.3424	
Au-PS (in air)	10.7	1.6056/1.5971	49.9/48.5
Au-PS-chitin(in air)	1790	1.3678/1.3651	26.2°/<1
AU-PS (in buffer)	5.5	1.6056/1.5971	N.D.
PS-Au-chitin (in buffer)	26.4	1.3379/1.3350	<1/<1[4]
	155.6	1.3357/1.3311	

(1) Contact angle was determined over a range of 60 seconds; the first measured angle is at 1 second, while the end value is the average of a stable angle between 45 – 60 sec. Values lower than 1° represent a flat or absorbed water droplet on the surface; (2) Plasma cleaned Au surface; (3) Au surface cleaned with NH_3 (30%)/H_2O_2 (30%)/H_2O (1:1:5, v/v) oxidizing solution; (4) Chitin surface was washed and dried under a nitrogen flow with buffer B.

533

534 Table 2. Kinetic binding properties to chitin and CBD-split intein.

Protein	SPR Surface	KD_1 [nM]	KD_2 [nM]	B_{max2}/B_{max1}[1]
CBD-IN_N	Au-Chitin	76.3	0.0425	0.29
CBD-IN_N	Au-PS-Chitin	< 0.001[4]	0.0052	0.08
IN_C-eGFP	Au-Chitin + 0.025 nM[2] CBD-IN_N	90.3	0.0026	0.18
IN_C-eGFP	Au-Chitin + 0.25 nM[3] CBD-IN_N	42.5	< 0.001[4]	0.23
IN_C-eGFP	Au-PS-Chitin + 0.025[2] nM CBD-IN_N	13.8	0.0571	0.40
IN_C-eGFP	Au-PS-Chitin + 0.25[3] nM CBD-IN_N	1.63	0.0509	0.48

535 (1) B_{max2}/B_{max1} is the ratio of non-specific binding over specific binding; (2) 0.5 µg/ml; (3) 5 µg/ml;

536 (4) Upper limit for affinity, as precision in fits cannot be obtained due to the limited dissociation of

537 these samples.

538

539

540

541 Table 3. Selection of CBD and their binding characteristics with chitin.

Species	**Domain name**	**Kd**	**Method**	**Ref**
Serratia	CBP21	1.4 µM	Solution depletion method	Vaaje-Kolstad *et al.*

marcescens				2004 [41]
Bacillus thuringiensis serovar *kurstaki*	*Bt*CBD	5.25 μM[1] (α-form) 3.46 μM (ß-form)	Solution depletion method	Manjeet *et al*. 2013 [42]
B. licheniformis DSM13	*Bl*CBD	5.98 μM[1] (α-form) 4.12 μM (ß-form)	Solution depletion method	Manjeet *et al*. 2013 [42]
Spodoptera litura multicapsid nucleopolyhedrovirus	GP37	0.061 μM	Solution depletion method	Li *et al*. 2003 [43]
Bacillus circulans	CBD_{ChiA1}	N.D. (K_r = 14.9 L/g)	Solution depletion method & ITC[3]	Hashimoto *et al*. 2000 [44]
Bacillus circulans	CBD_{ChiA1}	1.05 μM	Solution depletion method	Hardt and Laine 2004 [45]
Bacillus circulans	CBD_{ChiA1}	76.3 nM	SPR (Au-Chitin)	*This study*
Bacillus circulans	CBD_{ChiA1}	< 0.001[4]	SPR (Au-PS-Chitin)	*This study*

(1) B_{max} values of *Bt*CBP were 2.18 ± 0.53 μmol/g for α-chitin and 2.92 ± 0.29 μmol/g for β-chitin;

(2) B_{max} values of *Bli*CBP were 1.28 ± 0.007 μmol/g for α-chitin and 1.6 ± 0.18 μmol/g for β-chitin.

544 (3) CBD_{CHA1} did not bind to soluble chitinous substrates, only specific binding to insoluble chitin
545 was observed.
546 (4) Upper limit for affinity, as precision in fits cannot be obtained due to the limited dissociation of
547 these samples.
548
549 Table 4. Optical parameters for the layers used in the Layersolver software for figure 4.

Sensor	**Layer**	**d [nm]**	**n_r (670 nm)**	**n_r (785 nm)**	**k [RUI] (670 nm)**	**k [RIU] (785 nm)**	**Type**
Au	Prism	0	1.5202	1.5162	0	0	Standard
	Chromium	2.25	1.40148	2.11206	2.36163	1.40291	Standard
	Gold	50.88	0.20332	0.19791	3.384549	4.89071	Standard
	Air	0	1	1	0	0	Standard
Au-Chitin	Prism	0	1.5202	1.5162	0	0	Standard
	Chromium	3.37	3.5889	1.9545	1.44746	8.01544	Standard
	Gold	46.3	0.22395	0.26372	3.89604	4.90096	Standard
	Chitin	1910	1.39075	1.38845	0	0	Standard
	Air	0	1	1	0	0	Standard
Au-Chitin (lower limit)	Prism	0	1.5202	1.5162	0	0	Standard
	Chromium	3.18	1.6162	2.49777	2.27739	2.17001	Standard
	Gold	49.41	0.20042	0.20038	3.95704	5.03863	Standard
	Chitin	49.42	1.36168	1.36168	-0.019	-0.019	Standard
	Buffer	0	1.3342	1.332	0	0	Standard
Au-Chitin	Prism	0	1.5202	1.5162	0	0	Standard

(upper limit)	Chromium	3.18	1.6162	2.49777	2.27739	2.17001	Standard
	Chitin	49.41	0.20042	0.20038	3.95704	5.03863	Standard
	Gold	188.51	1.34628	1.3428	-0.034	-0.034	Standard
	Buffer	0	1.3342	1.332	0	0	Standard
Au-PS	Prism	0	1.5202	1.5162	0	0	Standard
	Chromium	1.75	1.66531	2.49949	5.13164	7.85818	Standard
	Gold	49.75	0.20195	0.1418	3.55135	4.47549	Standard
	Polystyrene	10.89	1.6	1.6	-0.06	-0.06	Linear
	Air	0	1.0003	1.003	0	0	Standard
Au-PS Chitin	Prism	0	1.5202	1.5162	0	0	Standard
	Chromium	1.09	4.5166	0.29287	-0.06537	1.7632	Standard
	Gold	50.88	0.2391	0.27063	4.08143	5.02307	Standard
	Polystyrene	5.5	1.6056	1.5987	0	0	Standard
	Chitin	1790	1.3678	1.3651	0	0	Standard
	Air	0	1.0003	1.0003	0	0	Standard
Au-PS-Chitin (lower limit)	Prism	0	1.5202	1.5162	0	0	Standard
	Chromium	0.19	-3.45785	0.57461	-6.98458	0.10471	Standard
	Gold	50.22	0.25187	0.26315	4.04329	5.03546	Standard
	Polystyrene	5.5	1.6056	1.5987	0	0	Standard
	Chitin	27.25	1.33795	1.33795	-0.027	-0.027	Standard
	Buffer	0	1.3342	1.332	0	0	Standard
Au-PS-	Prism	0	1.5202	1.5162	0	0	Standard

Chitin (upper limit)	Chromium	-0.22	6.18797	-4.27058	-3.45867	4.7062	Standard
	Gold	50.41	0.25157	0.25931	4.05202	4.99513	Standard
	Polystyrene	5.5	1.6056	1.5987	0	0	Standard
	Chitin	154.6	1.33574	1.33574	-0.04	-0.04	Standard
	Buffer	0	1.3342	1.332	0	0	Standard

Figures

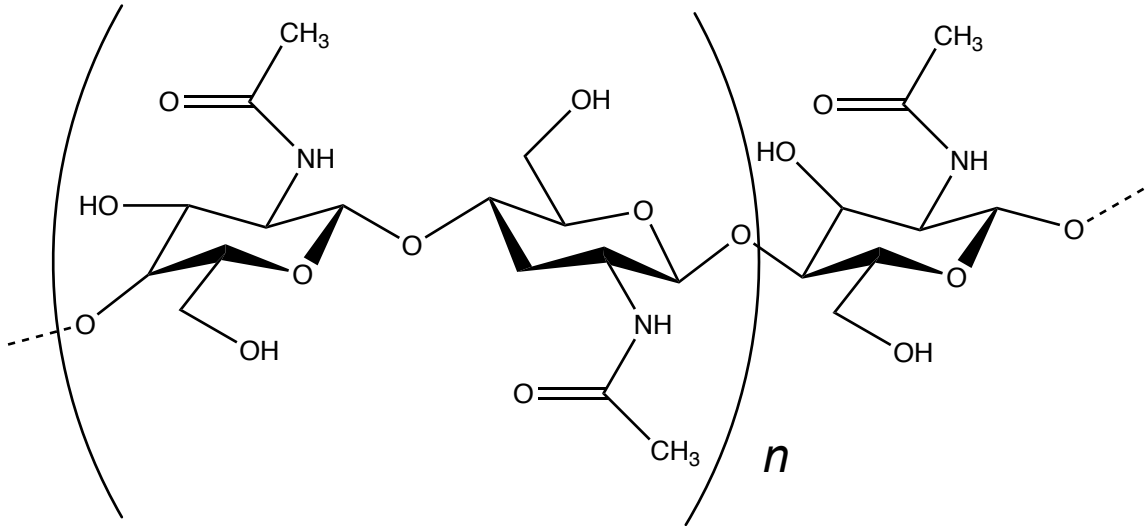

Figure 1. Chemical structure of chitin. Chitin polymers derived from shrimp shell have a typical degree of polymerization of 493 – 605 [46].

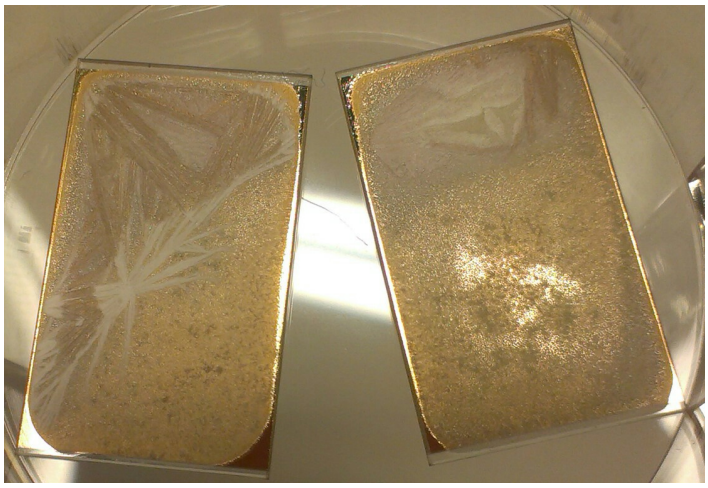

Figure 2. Au leaching of SPR chips due to LiCl in the 0.1% chitin DMA/5% LiCl solution. White areas are void of gold.

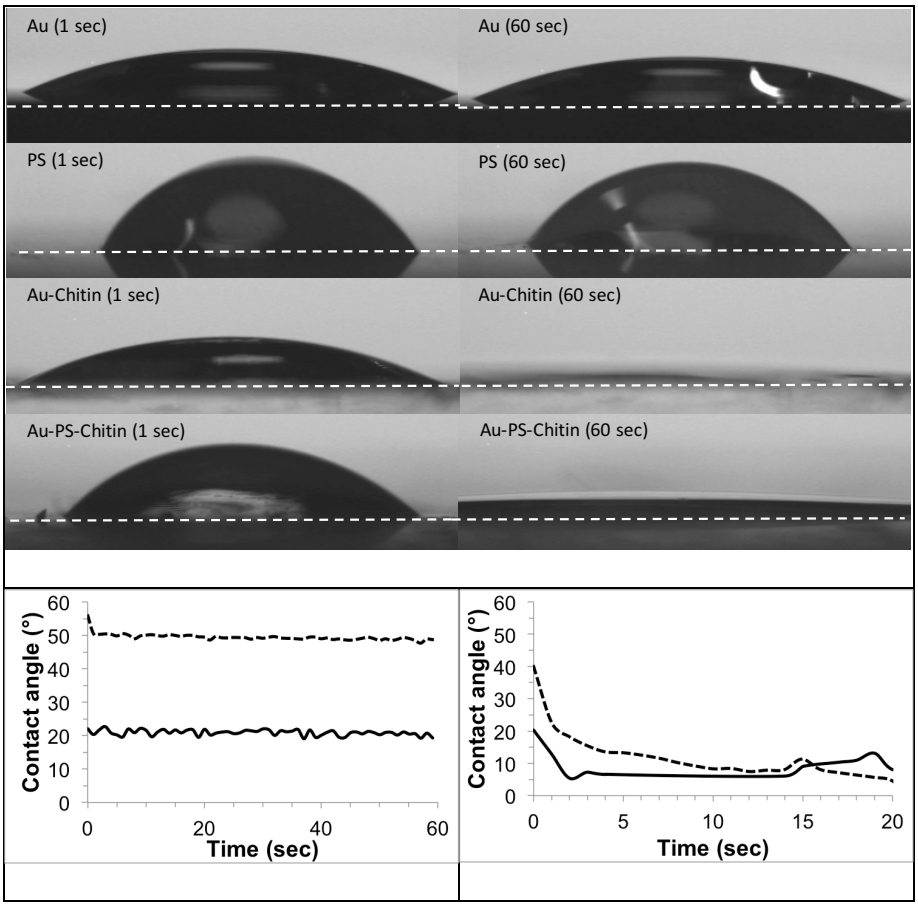

Figure 3. Water droplet behavior during contact angel measurements. The white dashed line in the upper panels depicts the droplet-surface interface. Droplets on Au (solid line) or Au-PS (dashed line) were stabile (bottom left), the droplet on dry Au-Chitin surface (solid line) reached a contact angle below 10° after 2 seconds, while the droplet on the dry Au-PS-Chitin surface (dashed line) reached a contact angle below 10° after 20 seconds (bottom right). All surfaces depicted here were plasma cleaned prior to measurements or spin-coating.

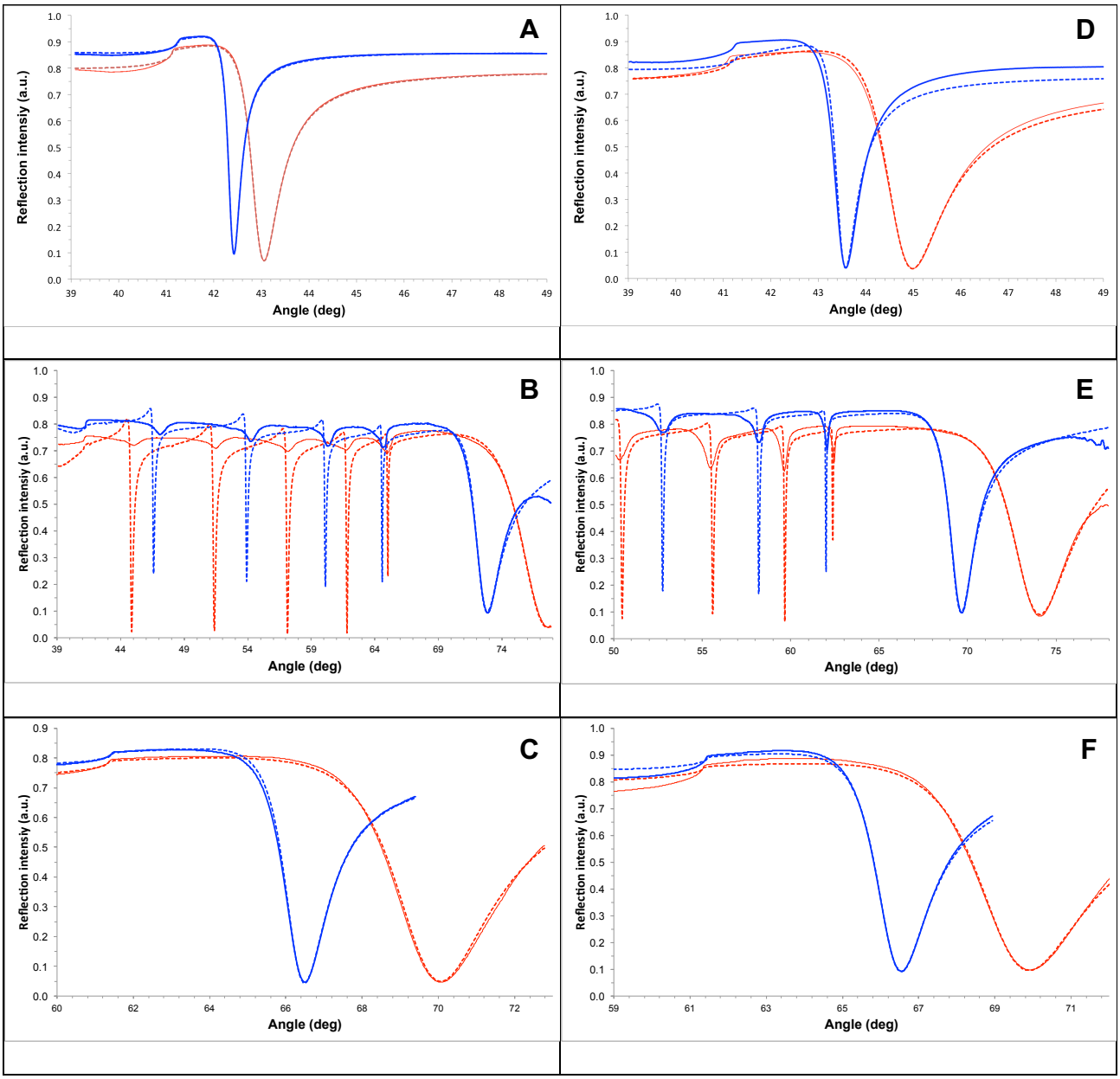

Figure 4. SPR full angle scans of (A) pure SPR sensor background, (B) spin-coated chitin on Au, (D) PS on Au, and (E) spin-coated chitin on PS on Au; 670 nm: red solid line, 785 nm: blue solid line with corresponding Layer solver fits (dashed lines). The optical parameters used for the Layer solver fitting are listed in table 4.

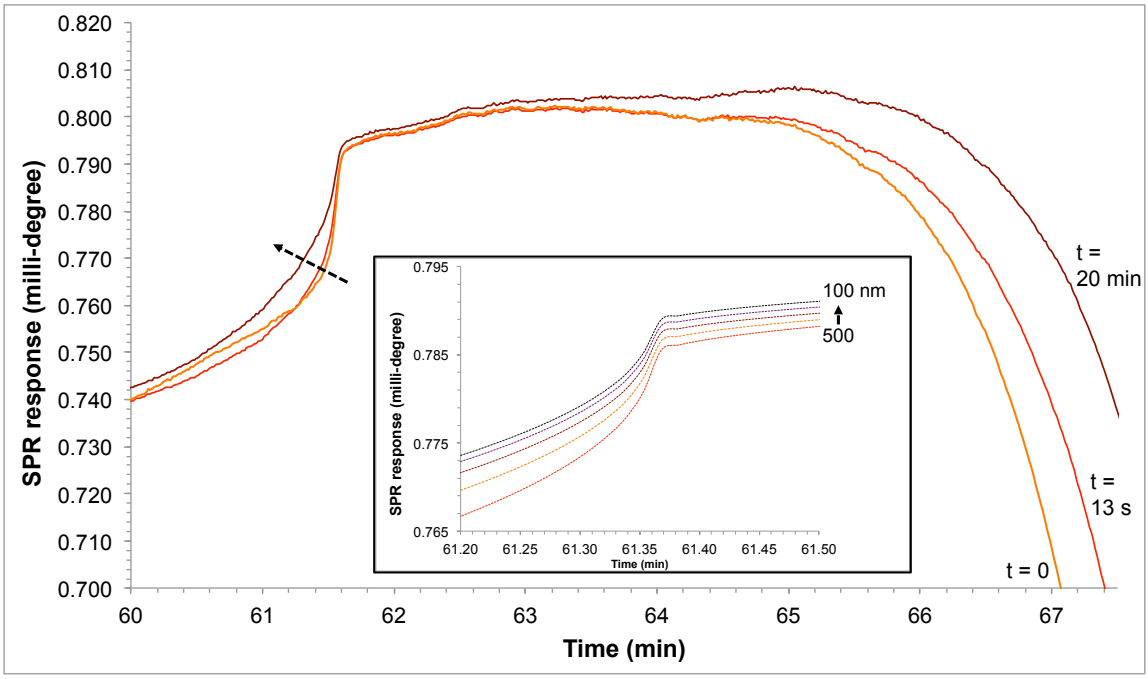

Figure 5. TIR detail of the full angle scans of spin-coated chitin on Au. For clarity the data derived from 670 nm is depicted, however the models were fitted for 670 and 785 nm simultaneously. In orange (t = 0) is the first time point after buffer B is introduced, in dark red (t = 20) the base line in the SPR sensorgram is stable. The dashed arrow indicates the shift of the shape of the TIR angle from thicker to a thinner layer. Inset: Layersolver model of the change of the TIR angle shape from 500 nm to 100 nm (chitin on Au).

582

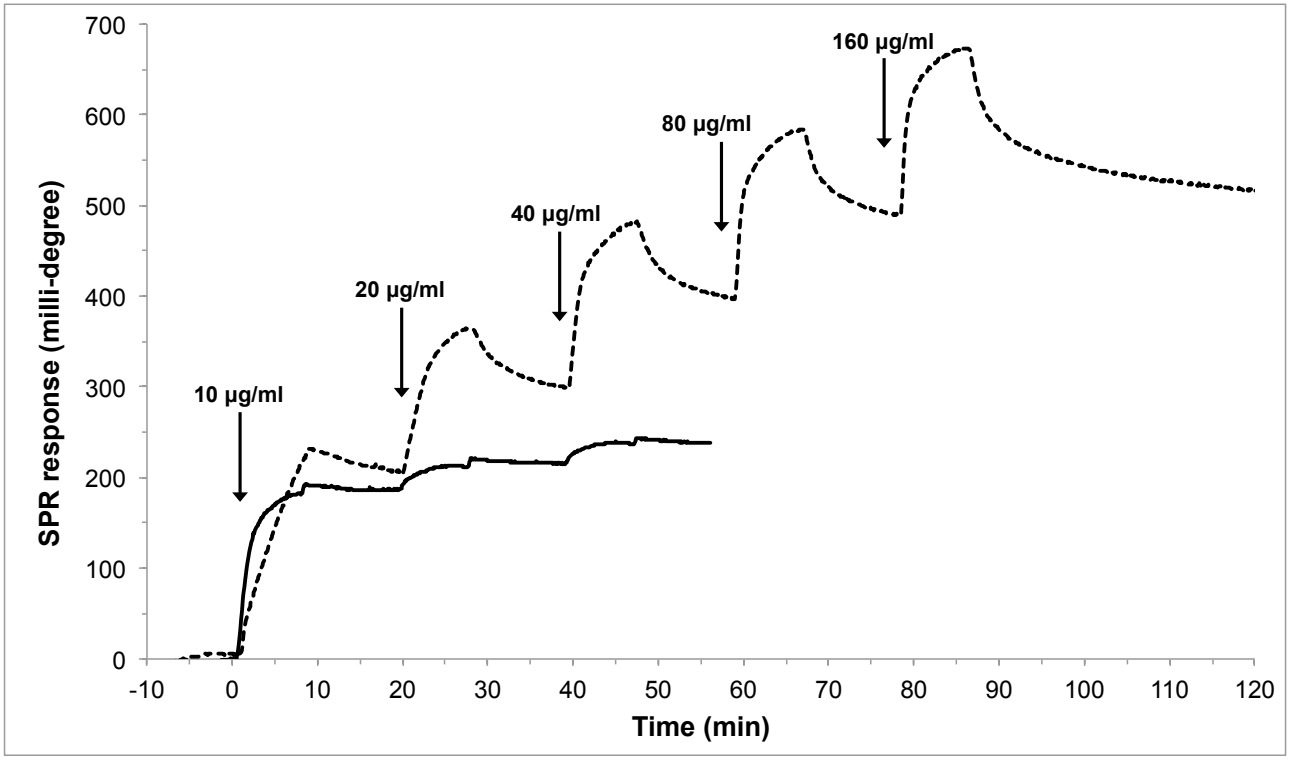

583 **Figure 6.** Titration of CBD-IN_N onto a spin-coated (SC) chitin layer on Au (dashed) or SC chitin

584 layer on PS (solid line). Concentrations are equivalent to 490, 981, 1961, 3922, and 7854 nM.

585

586

587

588

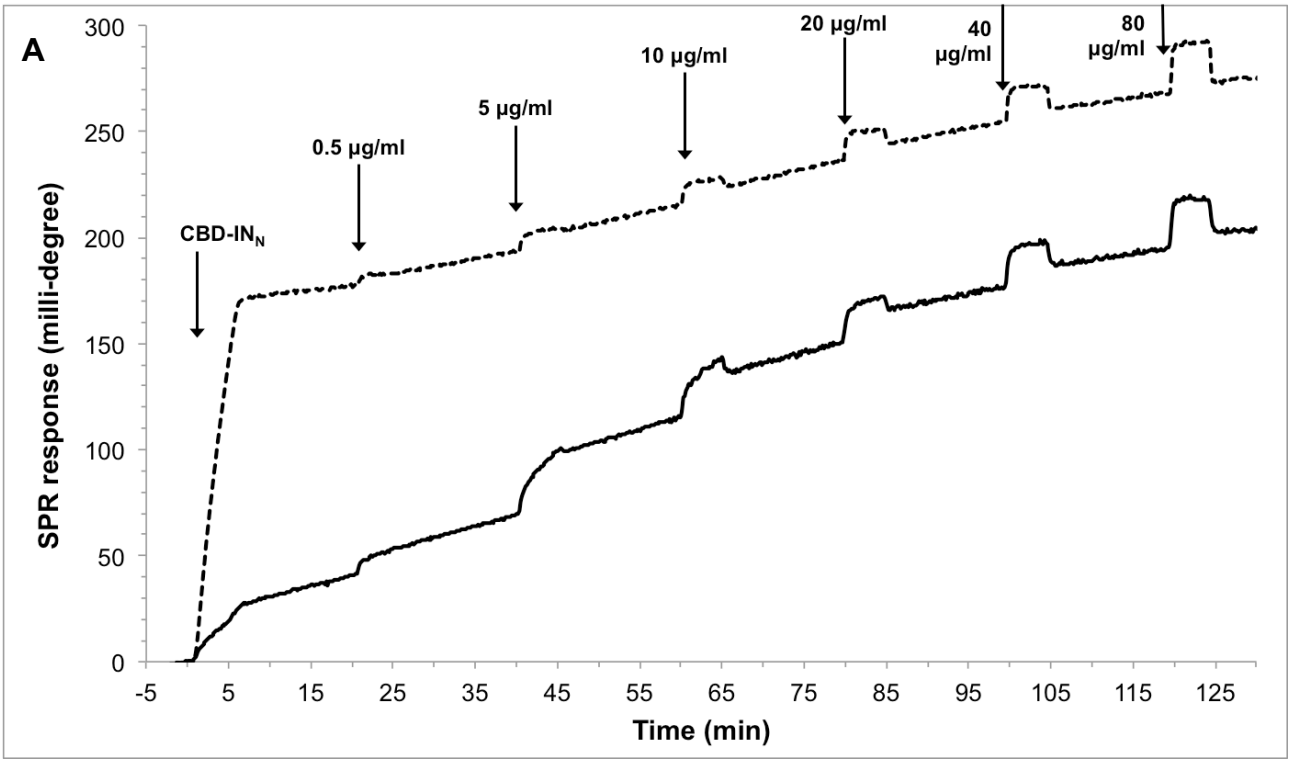

589

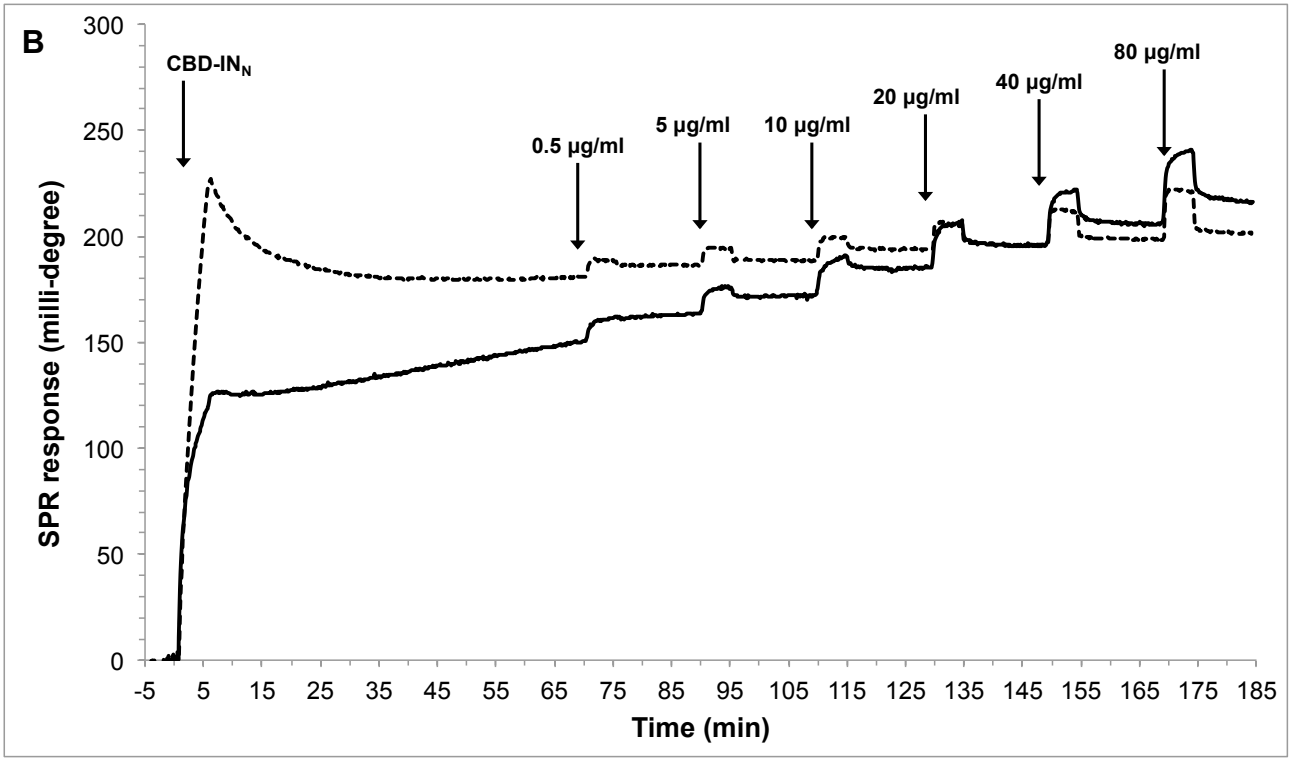

590

591 **Figure 7.** Titration of IN_C-eGFP onto a spin-coated chitin layer on (A) Au or (B) SC chitin layer on

592 PS after binding of 5 µg/ml CBD-IN_N (dashed lines) or 0.5 µg/ml CBD-IN_N (solid lines).

593 Concentrations are equivalent to 17.5, 175, 350, 701, 1401, 2803 nM.

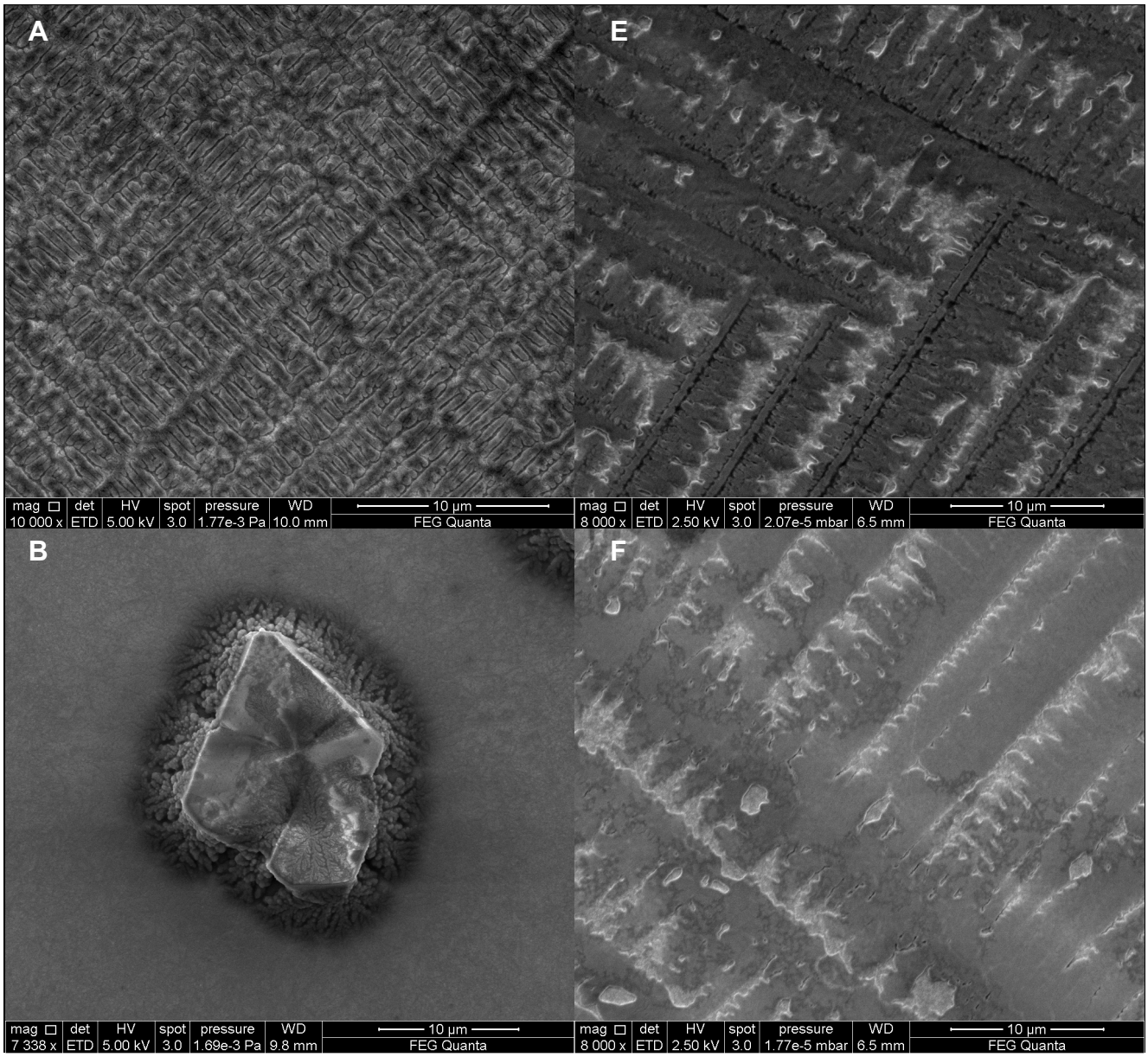
A
mag 10 000 x
det ETD
HV 5.00 kV
spot 3.0
pressure 1.77e-3 Pa
WD 10.0 mm
10 µm
FEG Quanta
E
mag 8 000 x
det ETD
HV 2.50 kV
spot 3.0
pressure 2.07e-5 mbar
WD 6.5 mm
10 µm
FEG Quanta
B
mag 7 338 x
det ETD
HV 5.00 kV
spot 3.0
pressure 1.69e-3 Pa
WD 9.8 mm
10 µm
FEG Quanta
F
mag 8 000 x
det ETD
HV 2.50 kV
spot 3.0
pressure 1.77e-5 mbar
WD 6.5 mm
10 µm
FEG Quanta

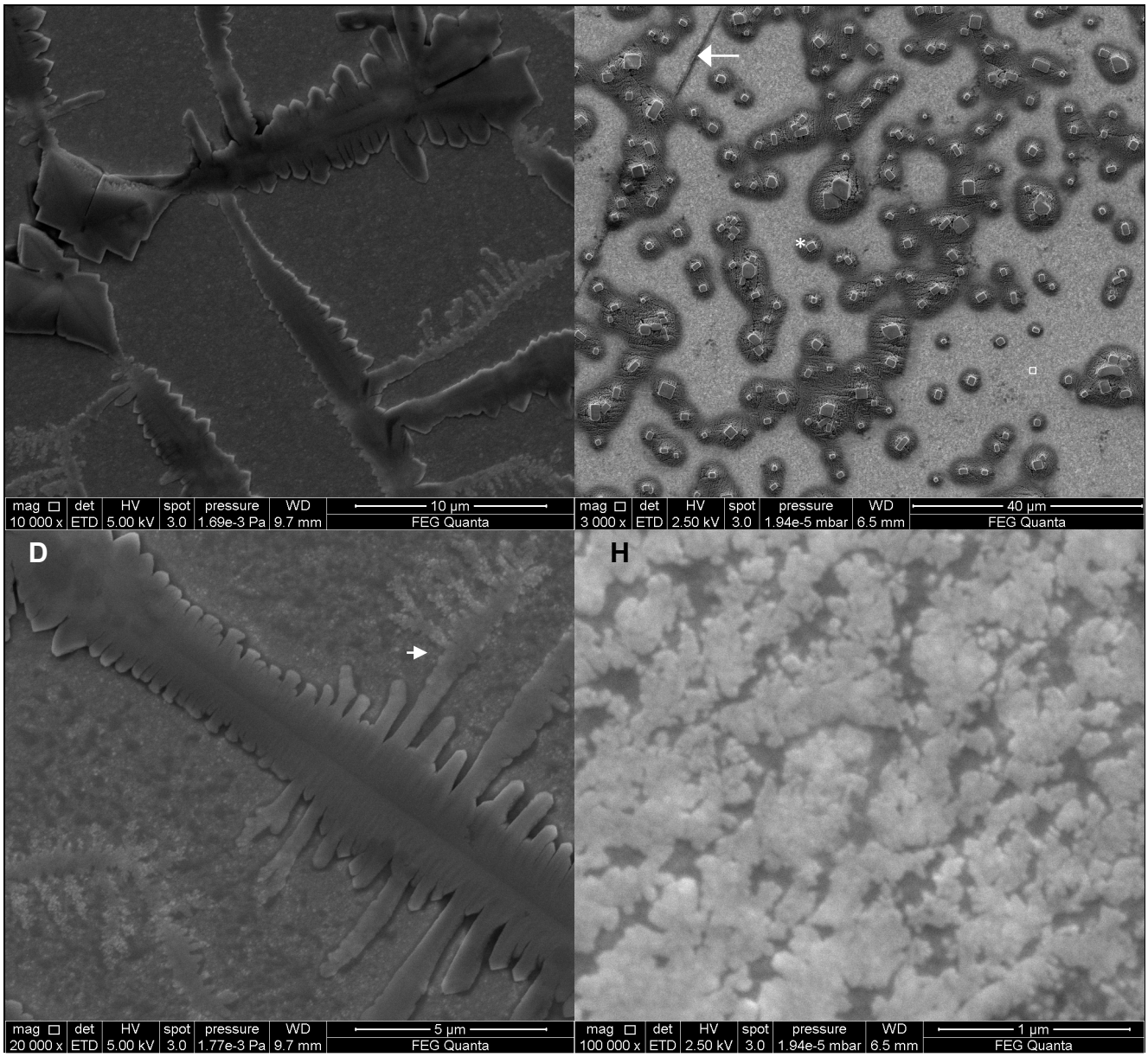

Figure 8. SEM images of the chitin surface (A) on Au in air (after 5 min), (B) on Au in air (after 1 hour), (C) on Au after 15 min of buffer B in the SPR flow cell (at 20 µL/min), and (D) as C, with higher resolution (arrow shows microstructure of chitin is attached to the macrostructure). (E) on Au-PS in air (5 min), (F) on PS in air (after 1 hour), (G) on Au-PS after 15 min of buffer B (at 20 µL/min); (*) cubic shapes are likely sodium chloride crystals; the arrow in F shows a line of non-coated Au, between two areas of PS coating; small white square in F the magnified area shown in G, and (H) as G, with higher resolution.

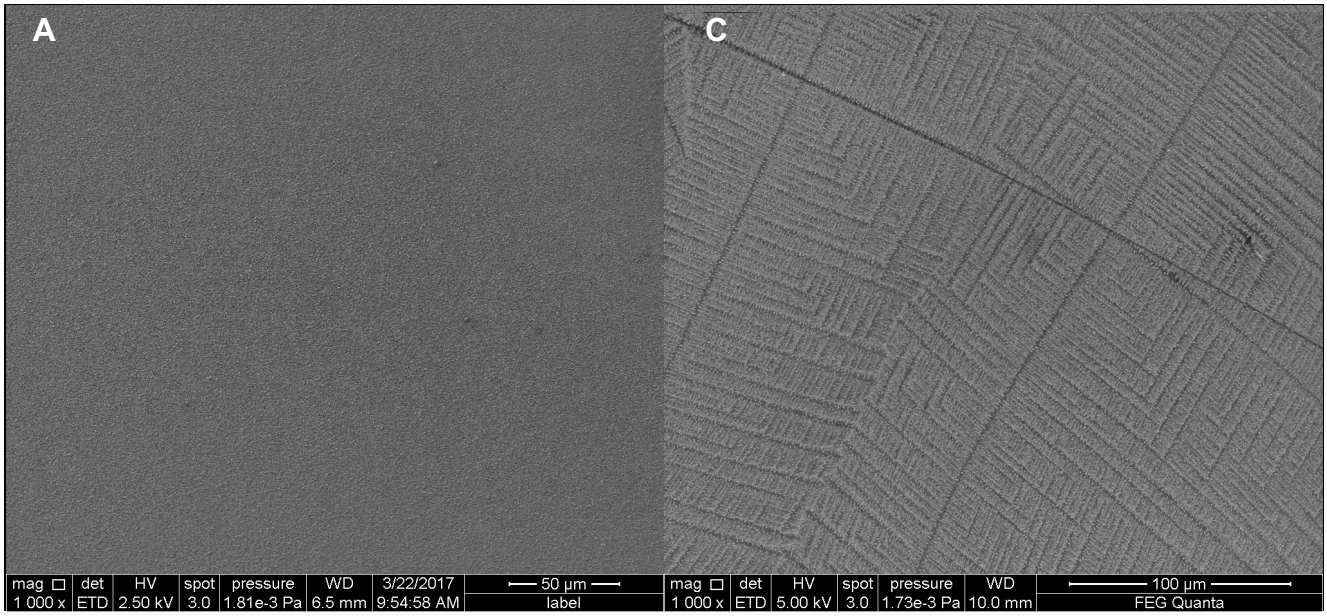
A
C
mag 1 000 x
det ETD
HV 2.50 kV
spot 3.0
pressure 1.81e-3 Pa
WD 6.5 mm
3/22/2017 9:54:58 AM
50 µm
label
mag 1 000 x
det ETD
HV 5.00 kV
spot 3.0
pressure 1.73e-3 Pa
WD 10.0 mm
100 µm
FEG Quanta

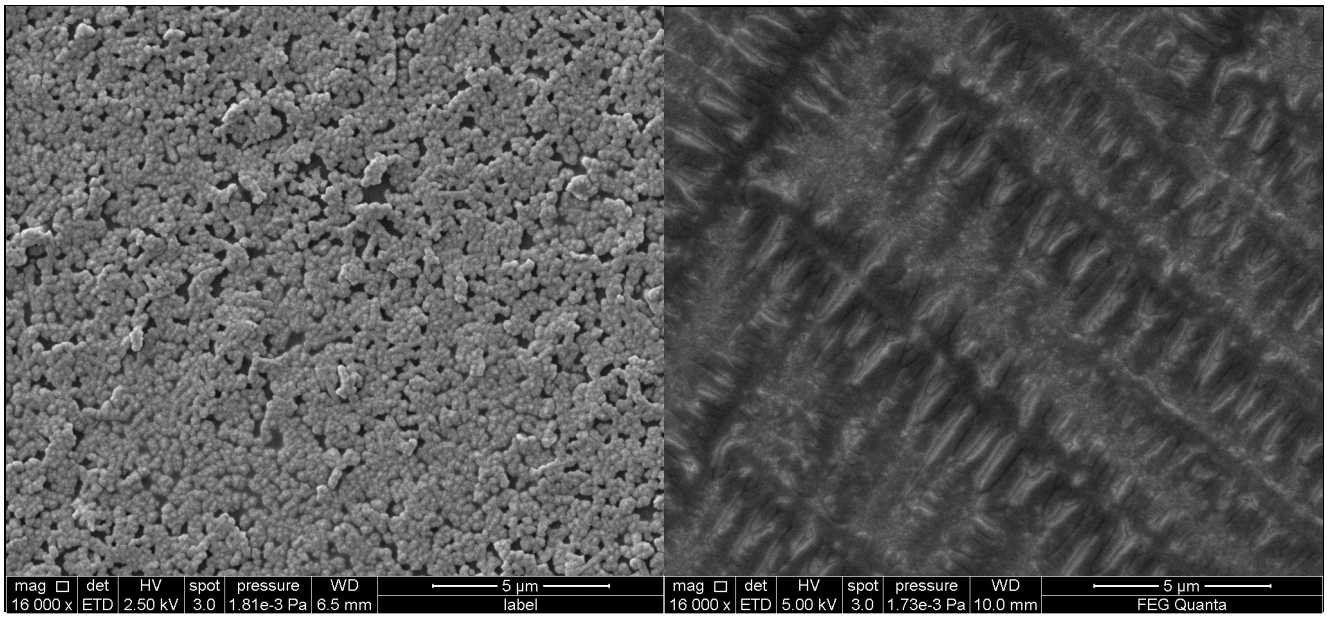

Figure 9. SEM images of chitin spin coated on Au-PS in air, after (A) < 30 seconds, (B) < 30 seconds at higher magnification, (C) 5 minutes, (D) 5 minutes at higher magnification.